QUANTUM SIMULATIONS USING NMR QUANTUM PROCESSOR

A thesis submitted towards partial fulfilment of
BS-MS Dual Degree Programme

by

SHARAD JOSHI

under the guidance of

DR. T.S MAHESH

Associate Professor
,Department of Physics,
IISER Pune

Indian Institute of Science Education and Research
Pune

Certificate

This is to certify that this thesis entitled "Quantum Simulations using NMR Quantum Processor" submitted towards the partial fulfilment of the BS-MS dual degree programme at the Indian Institute of Science Education and Research Pune represents original research carried out by "Sharad Joshi" at "IISER Pune", under the supervision of "DR. T.S Mahesh" during the academic year 2013-2014.

Student
SHARAD JOSHI

Supervisor
DR. T.S MAHESH

Acknowledgements

Foremost,I would like to express my sincere gratitude to my mentor Dr. T.S Mahesh for his continuous support and motivation during my MS research and study.Working under Dr. T.S Mahesh was a truly stimulating and intriguing experience.The most amazing quality of Dr. Mahesh is that he entertains even the vaguest of your ideas patiently and motivates you to pursue that idea.Every single conversation with him was a great learning experience for me. I am really lucky to have worked under Dr.Mahesh.

I would also like to thank Dr. M.S Santhanam for his useful advises and dicussions on Quantum Chaos.He was like my assistant advisor on this project.I would like to thank Dr. Anirban Hazra for his discussions on Franck-Condon principle and its quantum simulation.I am also indebted to Prof. Avinash Khare for his course in Quantum Mechanics and for the discussions on theory of quantum mechanics and SUSY.

Working in the NMR lab gave me the opportunity to meet some really talented people.I would like to thank Abhishek Shukla for helping me alot with the experiments(as I knew almost nothing about NMR experiments) and for all the discussions on various ideas that we had.I would like to thank Swathi,Deepak,Pooja and Pawan for all the chats academic/non-academic that we had.I would like to thank my friends Smriti,Pravu,Purvi,Prashant,Shirish and the whole basketball team for making my stay here at enjoyable and fun. Finally I would like to thank my family for all their support and advises on worldly matters.

Abstract

Quantum simulations are theorized to be much more efficient than the classical simulations. In this thesis,we tried to simulate(quantum mechanically) two different problems -
1)The statistical properties of "quantum chaos" in kicked rotor system are studied and numerically simulated.All the simulations are done using 8-qubits on MATLAB.
2)Franck-Condon factors (FCFs) play an important role in understanding many vibronic transitions occurring during molecular photoexcitations.In this article, we describe two general methods for estimating FCFs using a quantum information processor. We also illustrate the methods by experimentally estimating FCFs with the help of a three-qubit NMR quantum information processor.We were also able to show *quantum tunneling* as a byproduct of estimating FCFs.As can be seen in the corresponding section,the experimental results are in really good agreement with the theory.

List of Publications

1. **Estimating Franck-Condon Factors using 3-Qubit NMR Quantum Processor** (*In writing*)

Contents

1 Introduction **3**

2 Quantum Chaos **6**
2.1 Theory 6
2.1.1 Universal Signatures of Chaos 7
2.2 Kicked Rotor/Rotator 8
2.2.1 Classical model 8
2.2.2 Quantum Model 9
2.3 Numerical Simulations 11
2.3.1 Quantum Suppression of Classical Chaos 11
2.3.2 Fidelity Decay as a Signature of Chaos 12
2.3.3 Probability Distribution of Level Spacing 13

3 Estimation of Franck-Condon Factors using NMR **15**
3.1 Theory 15
3.2 Estimating FCFs by Using Method 1 17
3.2.1 An extention to Moussa Protocol 18
3.2.2 Simulations and Experiment 19
3.3 Estimating FCFs using Method 2 23
3.3.1 Experiment 24
3.4 Conclusion 24

References **26**

A Proofs **28**
A.0.1 Finding expectation value of a general unitary operator using Moussa protocol 28
A.0.2 Extracting expectation value of a Hermitian operator compatible with a pure-state 28

Chapter 1

Introduction

In early twentieth century people start realizing that physics (classical physics) as they know, is not quite accurate, as many absurd prediction were made by the physical theories e.g U-V catastrophe involving infinite energies, lack of explanation for stability of an atom (classical physics predicts that electrons spiral into the nucleus) etc. This leads to the birth of a new physical theory (Quantum Mechanics) after careful research for a quarter century. Since that time Quantum mechanics has been tested and applied to almost everything from structure of atoms, theory of radiation to elementary particles of nature to nuclear fusion in stars and Sun with high success. Now it has become a second nature to every person doing Science.
Since INFORMATION IS PHYSICAL - ROLF LANDAUER and physics as we know now is quantum in nature it is obvious to try to study information processing tasks using principles of quantum mechanics. This leads to the birth of quantum computation and information devoted to a big dream of realizing quantum computers which are much much more powerful and efficient than their classical parts. Here efficient means if the problem can be solved in polynomial time using polynomial resources. Two important aspects of Quantum mechanics which have no classical counter parts are

1) Entanglement, and

2) Superposition.

These are the two main properties of quantum systems, responsible for exponential speed up over classical systems[12]. The first step towards proving that Quantum Computers might be more powerful than classical ones was taken by David Deutsch in 1985 by constructing a toy problem which can be solved exponentially faster in quantum regime than in classical regime. This

revolutionary idea was further corroborated by Peter Shor's Algorithm(1994) which can solve the 'Prime factorization problem' and 'Discrete Logarithm problem' exponentially faster on a quantum computer, Grover's Search Algorithm(1995) which gives Quadratic speed up over classical algorithms, Seth Lloyd's Algorithm for solving a system of linear equations. These algorithms attracted a lot of attention as these problems are still not solvable (efficiently) on classical computers. In 1982 Feynman correctly mentioned, pointing out that doing simulation of quantum mechanical problems on classical computers is not efficient and sooner or later we might hit a wall in this field, '*Nature isn't classical dammit, and if you want to make a simulation of nature, you'd better make it quantum mechanical, and by golly it's a wonderful problem because it doesn't look so easy*'. In 1990s People started developing this idea of quantum simulation using quantum computer and showed that using quantum computers it is indeed possible to perform efficient simulations of problems which have no known efficient classical simulation, again proving that Quantum computers might be tremendously more powerful than classical ones.

Divincenzo gave 5 necessary and sufficient criterias for a system to be a perfect quantum computer [13].Many quantum systems are shown to satisfy several (not all) of these criterias e.g. NMR, Ion Traps, SQUIDS, Optics and photons, Optical cavities etc. NMR involves manipulating and measuring/detecting nuclear spin states using RF electromagnetic pulses. In 1997, the concept of pseudo pure states in NMR was discovered and since that time NMR has played a leading role in practical implementation of quantum information and computation by implementing almost all quantum algorithms e.g. Shor's algorithm using 7 qubit NMR processor, Grover's Search Algorithm, quantum error correcting codes, quantum logic gates, Quantum Simulations etc. Since nuclear magnetic moment is very small therefore we need a large number of molecules to get a detectable signal and therefore NMR uses an ensemble of molecules which makes it difficult to control and manipulate. Nuclear Spins are ideal candidates for building a Quantum computer but LIQUID-STATE NMR technique has two major drawbacks [18] -

1) It is not scalable as it suffers an exponential loss of signal with increasing number of qubits. So it can be used as a test bed for Quantum Computing at a smaller scale but can't be used to build large-scale quantum computer.

2) Preparation of an arbitrary initial pure state is really difficult owing to the very small energy gap between the nuclear states at thermal equilibrium.

As RF pulses are quite accurate in implementing unitary operators and can

be used to implement universal quantum logic gates, NMR has proven itself to be a really precise quantum information processor. In this study, we worked on the problem of quantum simulation of Quantum chaos in chapter 2,successful NMR implementation of Franck-Condon principle and Quantum tunneling in chapter 3 and now working on using SUSY to experimentally find the wave functions of Hydrogen atom by performing a quantum simulation.

Chapter 2

Quantum Chaos

2.1 Theory

The term 'Quantum chaos' corresponds to 'quantum study of systems whose classical analog exhibit chaotic behavior'. Classically, Chaos is formulated as extreme sensitivity to initial conditions i.e. two arbitrarily nearby initial points in phase space will diverge exponentially with time,if the system is chaotic. The rate of exponential divergence is quantified by the largest lyapunov exponent of the system: if it is positive then the system is chaotic. Now since classical physics is a limit of quantum physics, it's natural to study chaos quantum mechanically. In Quantum regime, since the Schrodinger equation is linear (it corresponds to no hypersensitivity to initial conditions) and also because of the hermiticity of the Hamiltonian the operators are unitary which implies that the overlap of two arbitrarily close initial states won't change with time.This implies the classical definition of chaos fails in quantum regime. Now the question arises: What does it mean to not have chaos quantum mechanically but classically? Is it that Quantum mechanics is wrong or the correspondence principle/Ehrenfest's principle is wrong? Ehrenfest's principle states that for large quantum numbers the average position and momentum in quantum regime should reproduce classical paths. Ehrenfest also showed that for the difference between the 2 averages (quantum and classical) to grow significantly (noticeable) is large enough for all experimental purposes. But it is only true for regular systems. For chaotic systems the time scale to notice the differences in quantum and classical predictions is too small.

2.1.1 Universal Signatures of Chaos

1. Probability distribution of level spacing: The statistical properties of quasienergy spectrum of quantum systems is highly universal.The distribution of spacing between the neighboring energy levels is a Wigner-Dyson distribution for a chaotic system i.e. $Se^{-\pi/4S^2}$the levels are highly correlated and they repel each other. This result comes from Random Matrix Theory[7]. In short, quantized chaotic systems show level repulsion while regular systems show level clustering with the PDLS as e^-S i.e. poissonian distribution. [17]
2. Fidelity decay as a signature of chaos: Peres observed that if instead of perturbing the initial state slightly, we perturb the governing Hamiltonian slightly and then measure the overlap of time evolution of 2 identical states under these 2 Hamiltonians, there is a characteristic exponential decay in case of chaotic systems, given the perturbation is sufficiently strong i.e. Consider an initial state $|\psi\rangle$ evolved under a unitary observable U i.e. $|\psi_u\rangle = U^n|\psi\rangle$, n being the number of iterations. Consider another operator U_p which is slightly perturbed from the operator U. Then the evolution of $|\psi\rangle$ under this operator is $|\psi_p\rangle = U_p^n|\psi\rangle$.The fidelity provides the divergence between these two states.

$$F(n) = |\langle\psi_p|||\psi_u\rangle|^2 \tag{2.1}$$

It will be exponentially decaying in case of chaotic systems [5]

3. In case of kicked rotor, there's one property that arises only because of quantum treatment of the problem i.e. 'Quantum suppression of classical chaos'. Here the variance of momentum, hence energy, in classical regime increases linearly with time while in quantum regime energy initially follows classical plot but then saturates after a break time. An intuitive picture of why this happens can be described as: Kicked rotor system is related to one-dimensional Anderson Model where a particle can hop from site to site. In Anderson's model, applying Furstenberg's theorem[7] we get that all eigenstates of this Hamiltonian are localized at the sites. From here one can reason that the eigenstates of the kicked rotor system are also exponentially localized in momentum space, as the role of momentum in kicked rotor is played by sites in Anderson's model. Now if we consider an initial wave function localized with some finite width in momentum space, then we can say that it overlap significantly only with some finite number of eigenstates and the overlap is exponentially small for all states outside its initial width. Since the overlap with an eigenstate is constant over time, as can be seen from Schrodinger equation, this implies the time evolution of the initial wave

function is restricted in momentum space. Therefore one can conclude that initially it'll spread like in classical case but after some time (break time), it will stop spreading. An in-depth description of this process is given in [17] [9]. In the next section we present the theory of kicked rotor in quantum and classical regime.

2.2 Kicked Rotor/Rotator

Kicked Rotor describes a particle constrained to move on a ring or a rotating stick while experiencing homogenous kicking at fixed interval of time.

2.2.1 Classical model

The hamiltonian for the system is-

$$H = p^2/2I + k\cos\theta\delta_T(t) \tag{2.2}$$

where p is the angular momentum,I is the moment of inertia and k is the kick strength and

$$\delta_T(t) = \sum_{n=-\infty}^{\infty} \delta(t - nT) \tag{2.3}$$

where T denotes the time period of the kick and n is an integer. We know from classical mechanics that given a Hamiltoonian *H(x,p)* the equations of motion are given by -

$$\frac{dx}{dt} = \frac{dH}{dp} \tag{2.4}$$

$$\frac{dp}{dt} = -\frac{dH}{dx} \tag{2.5}$$

this implies the equations of motion for one time interval T are

$$\frac{d\theta}{dt} = \frac{dH}{dp} \tag{2.6}$$

$$\theta_{n+1} - \theta_n = Tp_{n+1} \tag{2.7}$$

$$\theta_{n+1} = \theta_n + Tp_{n+1} \tag{2.8}$$

$$and \tag{2.9}$$

$$\frac{dp}{dt} = -\frac{dH}{d\theta} \tag{2.10}$$

$$p_{n+1} - p_n = k\sin\theta_n \tag{2.11}$$

$$p_{n+1} = p_n + k\sin\theta_n \tag{2.12}$$

At first,it seems like the equation of motion depends on 2 different parameter k and T, but if we just define K = kT, the equations will become

$$\theta_{n+1} = \theta_n + P_{n+1} \tag{2.13}$$
$$P_{n+1} = P_n + K \sin\theta_n \tag{2.14}$$

This is also known as standard map or chirikov-taylor mapping in nonlinear dynamics.This map has been studied thoroughly in nonlinear dynamics and here we'll mention some of its properties[2] without proving it.

1. The phase space of this mapping is a cylinder with bounded motion in θ but unbounded motion in P. It can also be seen that this map is periodic in P with a period of 2π.
2. When K=0 i.e. no kicking, then the phase space is a collection of straight lines with constant P. As we slowly increase K, the phase space lines starts to bend and after a critical value the phase space starts becoming chaotic(if the initial points are not in region of quasiperiodic motion).For kicked rotor,$K_{cr} = 0.9716$. If we keep on increasing $K > K_{cr}$ the regions of quasiperiodicity reduces and after some point the whole phase space become chaotic.
3.Our map is diffusive in P space. It can be shown like this

$$P_{n+1} = P_n + K \sin\theta_n \tag{2.15}$$
$$(P_n - P_0)^2 = K^2 \sum_{j,m}^{n-1} \sin\theta_j \sin\theta_m \tag{2.16}$$

Now if we consider a large number of trajectories with uniformly distributed θ and initial momentum $P_0 = 0$ The average momentum will be

$$\langle P_n^2 \rangle = K^2 n \tag{2.17}$$

i.e. it depends linealy on the number of kicks applied. Therefore in classical case the energy keeps on increasing with the applied number of kicks. In the next section we provide the details for quantum model of kicked rotor. [9]

2.2.2 Quantum Model

Here the hamiltonian is

$$H = -\frac{\hbar^2}{2I}\frac{d^2}{d\theta^2} + k\cos\theta\delta_T(t), \tag{2.18}$$
$$where, \quad \delta_T(t) = \sum_{-\infty}^{\infty} \delta(t - nT) \tag{2.19}$$

$\hbar$ is the reduced planck's constant and k is the kickstrength. Applying Schrodinger's equation,

$$i\hbar\frac{d\psi}{dt} = -\frac{\hbar^2}{2I}\frac{d^2\psi}{d\theta^2} + k\cos\theta\delta_T(t)\psi \tag{2.20}$$

this implies

$$\psi(\theta, t+T) = U\psi(\theta, t) \tag{2.21}$$

$$where, \quad U = \exp(-i\int_t^{t+T} H dt) \tag{2.22}$$

By applying Trotter's approximation we get,

$$U = \exp(iT\frac{\hbar}{4I}\frac{d^2}{d\theta^2})\exp(-ik\frac{\cos\theta}{\hbar})\exp(iT\frac{\hbar}{4I}\frac{d^2}{d\theta^2}) \tag{2.23}$$

$$\tag{2.24}$$

This is the time evolution operator over one period of time T. Here we can redefine our parametrs as

$$\tau = \frac{T\hbar}{I}, \quad k = \frac{k}{\hbar} \tag{2.25}$$

$$\therefore, \tag{2.26}$$

$$U = \exp(i\frac{\tau}{4}\frac{d^2}{d\theta^2})\exp(-ik\cos\theta)\exp(i\frac{\tau}{4}\frac{d^2}{d\theta^2}) \tag{2.27}$$

$$here, U_p = \exp(i\frac{\tau}{4}\frac{d^2}{d\theta^2}) \quad and \quad U_\theta = \exp(-ik\cos\theta) \tag{2.28}$$

Unlike in classical case where the dynamics depends on 1 parameter $\boldsymbol{K}$ only ,here we have 2 independent parameters τ and $\boldsymbol{k}$. We can call $\boldsymbol{k}$ to be a purely quantum parameter.The relation between classical and quantum parameters is given by

$$K = k\tau \tag{2.29}$$

We can express our wavefunction in the eigenbasis of unperturbed($k = 0$) kicked rotor hamiltonian

$$\psi(\theta, t) = \sum_{-\infty}^{\infty} A_m(t)e^{im\theta} \tag{2.30}$$

The most efficient way(in term of minimizing the time) to simulate the time evolution of our wavefunction is by using quantum fourier transform(QFT).Since

U_p is diagonal in moementum basis,U_θ is diagonal in position basis and initial wavefunction is expressed in momentum basis,we can use QFT to define our overall evolution operator(for one time interval T) i.e.

$$U = U_p U_{QFT}^\dagger U_\theta U_{QFT} U_p \tag{2.31}$$

Using this operator,we can calculate the wavefunction as well as energy after every kick. Energy in this case is given by

$$E = \sum_{-N}^{N} |A_m|^2 \hbar^2 \frac{m^2}{2} \tag{2.32}$$

where, the basis consists of $2N + 1$ eigenfunctions of unperturbed kicked rotor(because of numerical simulation we have to truncate the basis at some point).

2.3 Numerical Simulations

In this section,we provide the numerical simulations done on quantum kicked rotor to explore the universal signatures of chaos. All the simulations are done using **8 qubits**.

2.3.1 Quantum Suppression of Classical Chaos

Here we get that the energy in quantum regime gets saturated after a break time as per the reason being explained in section 2.1.1.

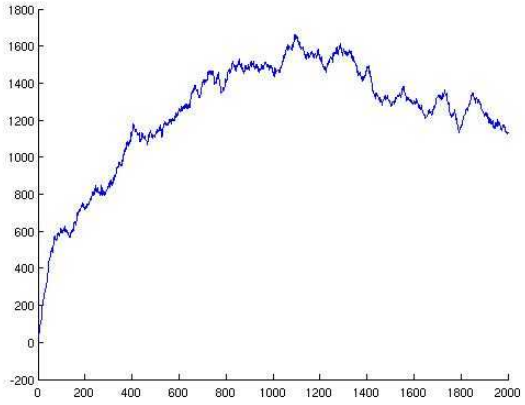

Figure 2.1: *Quantum suppression of classical chaos for* $k = 20$ *and* $\tau = \frac{1}{4}$, $\Longrightarrow$ *the classical parameter* $K = 5$.*Simulation was done on matlab using 8-qubits*

2.3.2 Fidelity Decay as a Signature of Chaos

Exponential fidelity decay can also be used as a signature of chaos. Here we simulated the quantum kicked rotor with two slightly different kick strength k_1 and k_2 figure2.2.

We have evolved the same state under these two different kick strengths

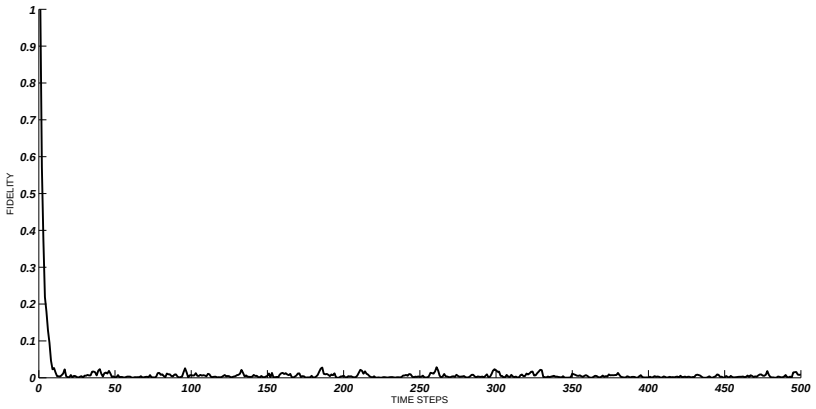

Figure 2.2: *Fidelity decay versus time steps.Here* $k_1 = 15$,$k_2 = 16.01$ *and* $\tau = 1/2$ *is used.Simulation was done on matlab with 8-qubits*

and measured the overlap between the two wavefunctions.

2.3.3 Probability Distribution of Level Spacing

As mentioned in section 2.1.1,probability distribution of level spacing can be used as an indicator of chaos. We expect to get Wigner-Dyson distribution for system in chaotic regime and poisson distribution for regular systems. Here, we present the numerial simulation of **PDLS** in case of kicked rotor

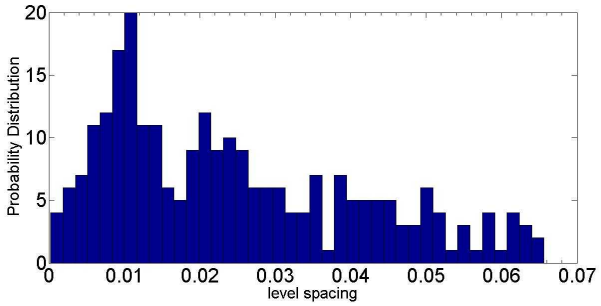

Figure 2.3: *Probability distribution of levelspacing in kicked rotor with* $k = 20$ *and tau* $= 1$ *this implies the classical parameter* $K = 20$*. Since the system is completely chaotic for* $K > 5$*,therefore we are clearly getting the Wigner-Dyson distribution here.*

in both chaotic and non-chaotic regime.We can clearly see that as we keep on decreasing K,the distribution becomes more and more poisson like as expected from RMT.

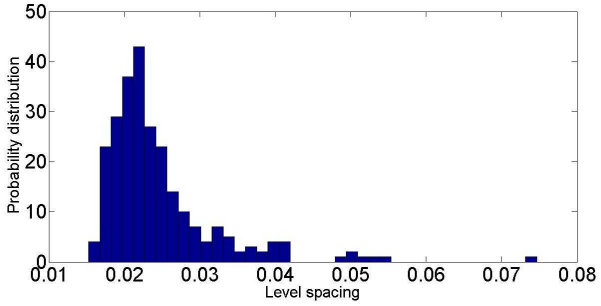

Figure 2.4: *Probability distribution of levelspacing in kicked rotor with* $k = 20$ *and tau* $= 1/4$ *this implies the classical parameter* $K = 5$*. Since the system is completely chaotic for* $K > 5$*,therefore we are clearly getting the Wigner-Dyson distribution here.*

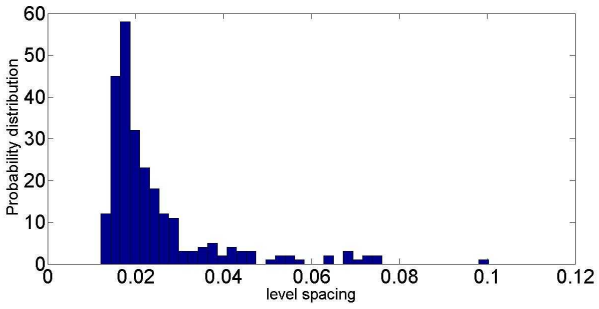

Figure 2.5: *Probability distribution of levelspacing in kicked rotor with* $k = 20$ *and tau* $= 1/5$ *this implies the classical parameter* $K = 4$*. Since the system partially chaotic for* $K < 5$*,therefore we are getting the poisson-like distribution here.*

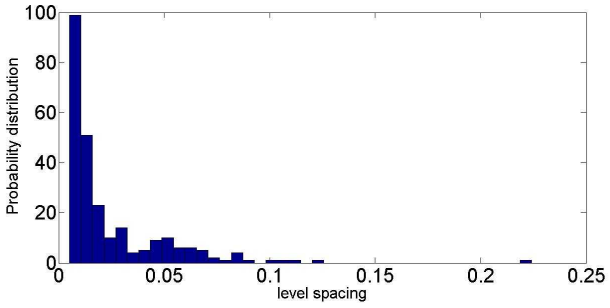

Figure 2.6: *Probability distribution of levelspacing in kicked rotor with* $k = 20$ *and tau* $= 1/10$ *this implies the classical parameter* $K = 2$*. Since the system partially chaotic for* $K < 5 and K > 0.9716$*,therefore we are getting the poisson-like distribution here.*

Chapter 3

Estimation of Franck-Condon Factors using NMR

3.1 Theory

Electronic transitions in molecules are often associated with vibrational transitions.Such combined transitions are known as *vibronic transitions* [8].Owing to its high mass,nuclear displacement is negligible compared to elctronic displacement,during a vibronic transition. Franck-Condon principle[4] states that the transition probability between 2 vibrational levels is given by the overlap between the respective wavefunctions [1].Franck-Condon factors play an important in understanding the vibronic transitions in photochemical reactions,photo-induced dissociations etc. In this work,we have used two different approaches(both of which gives arbirarily high spatial resolution of probability distribution) to estimate the Franck-Condon Factors(FCFs)-

Method 1) By using a 3 qubit NMR processor [3] we managed to estimate the FCF for all the transitions involving the ground state and the first 4 levels of Harmonic oscillator.We used Moussa Protocol(to extract the expectation values) and translation operator for this experiment. This method is very robust as shown in the experimental results. We also managed to show ***quantum tunneling*** in this experiment.

Method 2) By using a 3 qubit NMR processor we managed to estimate the FCF for all the transitions involved in first 4 levels of Harmonic oscillator.Diagonal Tomography is used in this approach.The experimental error is little higher than the first approach but with the same number of qubits we are getting much more information than the first method so it's efficient(in

terms of resources needed).

For low-lying vibrational levels,the smooth energy potential surfaces [4] can be approximated as simple harmonic oscillator. Here we model the lower vibrational levels as eigenstates of 2 harmonic osicllator,one corresponding to the electronic ground state(V_1) and other to excited elctronic state(V_2).

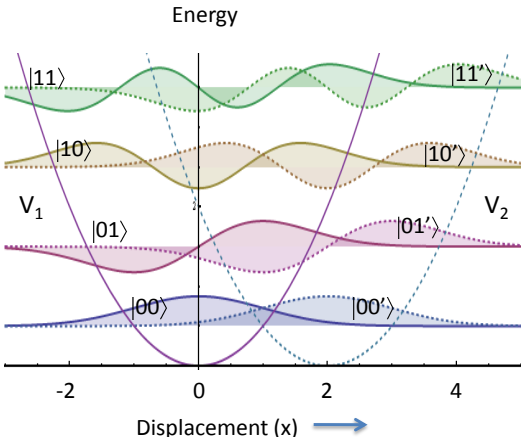

Figure 3.1: A harmonic potential centred at the origin (V_1), a displaced harmonic potential centred at $x = 2$ and with $\Delta E = 0$ (V_2), and their corresponding wavefunctions. The unshifted eigenfunctions are labelled in the computational basis and the shifted eigenfunctions are indicated with primes.

For convenience, we chose $V_1 = x^2/2$ and $V_2 = (x-b)^2/2 + \Delta E$. Now,in operator basis, $a = \frac{(x+ip)}{\sqrt{2}}$ and $a^\dagger = \frac{(x-ip)}{\sqrt{2}}$ [15]. Taking mass as well as angular frequency of the oscillator to be unity,the hamiltonian can be expressed as

$$\begin{aligned}
\mathcal{H}_1 &= p^2/2 + x^2/2 \\
&= a^\dagger a + 1/2 \quad \text{and,} \\
\mathcal{H}_2 &= p^2/2 + (x-b)^2/2 + \Delta E \\
&= (p^2/2 + x^2/2) + b^2/2 - xb + \Delta E \\
&= a^\dagger a + 1/2 + b^2/2 - (a + a^\dagger)b/\sqrt{2} + \Delta E, \qquad (3.1)
\end{aligned}$$

where $\hbar$ is set to unity.
For transitions between vibrational level $|m\rangle$ of electronic ground state and vibratinal level $|n'\rangle$ of electronic excited state,the transition probability$W_{m,n'}$ is

$$W_{m,n'} \propto f_{m,n'}(b) \qquad (3.2)$$

where,

$$\begin{aligned} f_{m,n'}(b) &= |\langle m|n'\rangle|^2 \\ &= \left| \int_{-\infty}^{\infty} \psi_m^*(x)\psi_{n'}(x,b)dx \right|^2. \end{aligned} \tag{3.3}$$

are known as Franck-Condon Factors(FCFs).Since we have chosen similar potentials with unit mass and angular frequency,FCFs depend on displacement b only. The separation in energy ΔE affects only the proportionality constant in equation above and hence it's chosen to be zero for convenience.

3.2 Estimating FCFs by Using Method 1

Here,estimating FCFs ($f_{m,n'}$) is equivalent to measuring the expecation value of a projection operator $P_m = |m\rangle\langle m|$ after preparing the system in excited state $|n'\rangle$

$$f_{m,n'} = |\langle m|n'\rangle|^2 = \langle n'|m\rangle\langle m|n'\rangle \tag{3.4}$$

$$= \langle P_m\rangle_{n'} \tag{3.5}$$

The preparation of state $|n'\rangle$ can be achieved by first preparing the corresponding electronic ground state $|n\rangle$ and translating it in position basis to desired displacement $x = b$. The translation operator for this purpose is

$$U_T(b) = e^{-ibP} \tag{3.6}$$

it can be discretized as

$$U_T^k(b/N) = e^{-ibPk/N} \tag{3.7}$$

achieving a displacement $\frac{bk}{N}$where $k \in \{0 \cdots N\}$

After preparing the initial state,the next step is to extract the expectation value of the involved observable A. The direct straightforwad way of doing that is to use quantum state tomography [12] to get the density matrix ρ and then evaluate the expectation value of A i.e. $\langle A\rangle_\rho = Tr(A\rho)$.But tomography requires large number of experiments as well as significant data processing [16]. An elegant and much simpler method for extracting expectation values of Unitary Observables(i.e. unitary as well as hermitian operator) was proposed bt Moussa et al [11]. It is described in the circuit diagram shown in fig 3.2a. It involves an ancilla initialized in $|+\rangle$ state and an initial state ρ. To measure the expectation value of the *unitary observable* A,we need

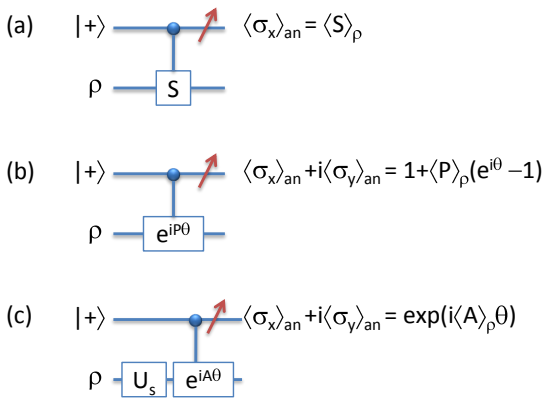

Figure 3.2: Circuits for Moussa protocol (a) and its extensions (b and c). In all the cases the top qubit corresponds to ancilla and the remaining are system qubits. In (b) P is a projection observable. In (c) the initial state ρ is a pure state and the observable A is compatible with it.

to apply the operator on the system controlled by ancilla and measure the expectation value of σ_x on ancilla.Then

$$\langle A \rangle_\rho = \langle \sigma_x \rangle_{ancilla} \tag{3.8}$$

In the next subsection we provide a simple extension of Moussa Protocol so that it can be used to extract the expectation value of any general observable.

3.2.1 An extention to Moussa Protocol

Consider a projection operator P with $P^n = P$. This operator is hermitian but not unitary, so, to make it unitary, consider $S = e^{iP\theta}$ to be our observable($\because$ exponential of a hermitian is unitary).Consider the circuit in fig.3.2a.It can be shown that

$$\langle \sigma_x \rangle_{\text{an}} = \langle S + S^\dagger \rangle_\rho / 2, \quad \text{and} \quad \langle i\sigma_y \rangle_{\text{an}} = \langle S + S^\dagger \rangle_\rho / 2,$$

so that

$$\langle \sigma_x \rangle_{\text{an}} + i\langle \sigma_y \rangle_{\text{an}} = \langle S \rangle_\rho = \langle e^{iP\theta} \rangle_\rho = 1 + \langle P \rangle_\rho (e^{i\theta} - 1),$$

and hence

$$\langle P \rangle_\rho = \frac{1 - \langle \sigma_x \rangle_{\text{an}}}{1 - \cos\theta}. \tag{3.9}$$

Taking $\theta = \pi$, we obtain $\langle P \rangle_\rho = (1 - \langle \sigma_x \rangle_{\text{an}})/2$.
Since any observable can be expressed as a summation of projection operators in some basis,and the expectation value of a sum is sum of expectation values of individual entries of that sum,we can extract the expectation value of any observable using extended Moussa Protocol(only the number of experiments will increase as per the dimension of our observable).

3.2.2 Simulations and Experiment

In numerical simulation,there's one inherent problem i.e. we have to truncate the basis at some finite level.Here are some numerical simulations of estimatimg FCFs with different number of qubits. For comparison,we have plotted the theoretical FCFs(for infinite level harmonic oscillator) also. We notice that with increasing number of qubits the simulaton results are in better agreement with the theory.

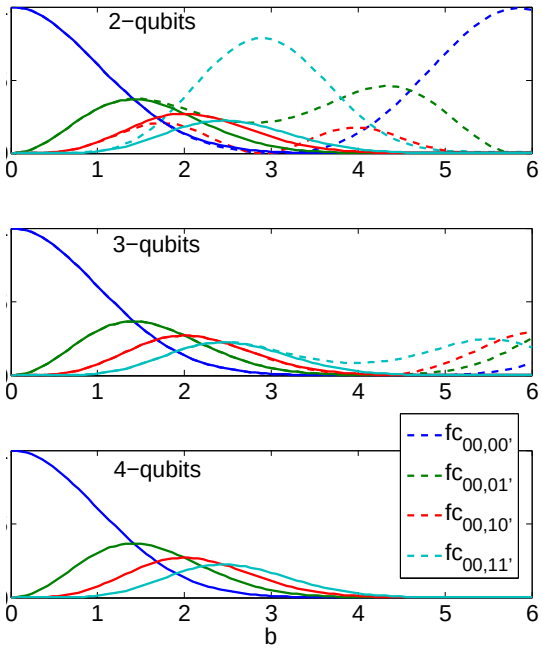

Figure 3.3: Simulation

Our expriment corresponds to the **2-qubit** simulation in Figure 3.3.We chose three spin-1/2 F_{19} nuclei of iodotriflouroethylene(C_2F_3I) dissolved in

acetone-D_6 as our 3-qubit NMR quantum processor.All the experiments are carried out on a 500MHz Brucker NMR spectrometer at an ambient temperatur of 300K. The molecular structure and the Hamiltonian parameters of our system is given in Figure 3.4.

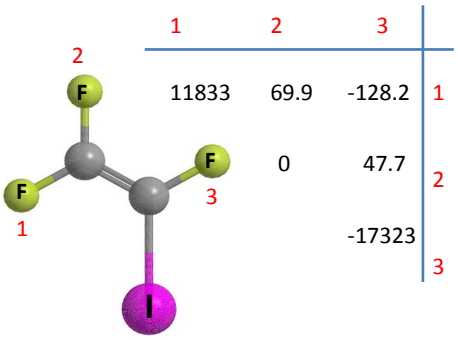

Figure 3.4: Molecular structure of iodotrifluoroethylene and its Hamiltonian parameters. The diagonal elements represent relative resonance frequencies and the off-diagonal elements represent the strengths of scalar (J) couplings.

In our experiment,We have selected F_1 (see Figure 3.4) as the ancilla qubit and the other two spins to encode the lowest 4-levels of the harmonic oscillator.The inital state was prepared,as explained above,by first preparing the corresponding state in electronic ground state and then translating it to the desired position(b) by using the translator operator ($U_T(b)$). Here, instead of initialiing the system in one single level we make use of "Pair of Pseudo Pure States"(POPS) [6] which initialies the system in a traceless psudopure mixture of two states
$\rho_{jk} = |j\rangle\langle j| - |k\rangle\langle k|$,where $j, k \neq j \in (|00\rangle, |01\rangle, |10\rangle, |11\rangle)$ After translation, the corresponding excited state is
$\rho_{j'k'} = |j'\rangle\langle j'| - |k'\rangle\langle k'|$.
In the experiment, we have chosen $P_{00} = |00\rangle\langle 00|$ as our observable.By using the approach in section 3.2.1,we found the overlap of $|00\rangle$ of electronic ground state with $|n'(b)\rangle$ of elctronic excited state with respect to variation in b.This way we can obtain the FCFs $f_{00,k'}$ with $j = |00\rangle$ and $k \in (|00\rangle, |01\rangle, |10\rangle, |11\rangle)$
The complete circuit for our simulation is given in Figure 3.5

Here,the first qubit is the ancilla and the other two are the system(encoding the harmonic oscillator).As described above,we first applied the translation

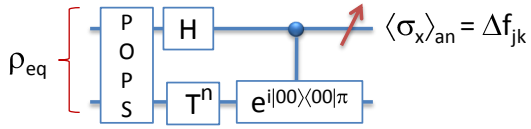

Figure 3.5: The overall circuit for estimating FCFs. The top qubit corresponds to ancilla and the remaining are system qubits.

operator $U_T^k = e^{-ib_m axkp/N}$ to prepare the excited state after preparing the initial state $|+\rangle\langle+| \otimes \rho_{jk}$. In our experiment $b_{max} = 4$ and $N = 11$.. The complete translation operator were realized using amplitude and phase modulated radio frequency pulses.These pulses were designed using GRadient Ascent Pulse Engineering(GRAPE) [10] technique with an average Hilbert-Schmidt fidelity of 0.995 over a spatial RF inhomogeneity in the range of 90% to 110% of the nominal field.After the translation,the operator $e^{iP_{00}\pi}$ on the system qubits controlled by ancilla qubit was applied (so that the overlap between $|00\rangle$ and the excited state $|n'(b)\rangle$ can be calculated as explained in section 3.2.1).The RF pulse designed via GRAPE for this operator had an average fidelity of 0.989 over the same RF inhomogeneity range as the translation operator.Finally the real part of the ancilla signal that is proportional to $\langle\sigma_x\rangle_{\text{an}}$ is measured by integrating the ancilla transitions. Thus after each preparation $\rho'_{j,k}$ we can extract the difference of FCFs $\Delta f_{j,k} = f_{00,j'} - f_{00,k'}$. In order to determine all individual FCFs of the form $f_{00,k'}$, we perform four different experiments and measure $\Delta f_{00,01'}$, $\Delta f_{00,10'}$, $\Delta f_{01,11'}$, and $\Delta f_{10,11'}$, and solve the four linear equations with the help of an additional constraint given by the normalization condition $\sum_j f_{00,j'} = F$.

The results of the experiment with $F = 1$ and for various values of $b \in [0, 4]$ are shown in Figures 3.6a and 3.6b. The experimental data points are shown by symbols. To understand the systematic errors in the experimental data, we have simulated FCF values using lowest four levels of the computational basis. In Figures 3.6 The simulated curves are shown by lines. Here a good agreement between the experimental results and the simulated curves can be observed. The good agreement between the experimental data points with the theoretically expected values confirm the successful measurement of FCFs. However, we have also shown the expected FCF curves for infinite level systems. As can be readily observed, while the FCF $f_{00,00'}$ shows a good agreement between the finite (4-level) and infinite cases, the profiles of other factors substantially deviate with the infinite case with increasing values of b. The deviation between the finite and infinite FCFs is due to the

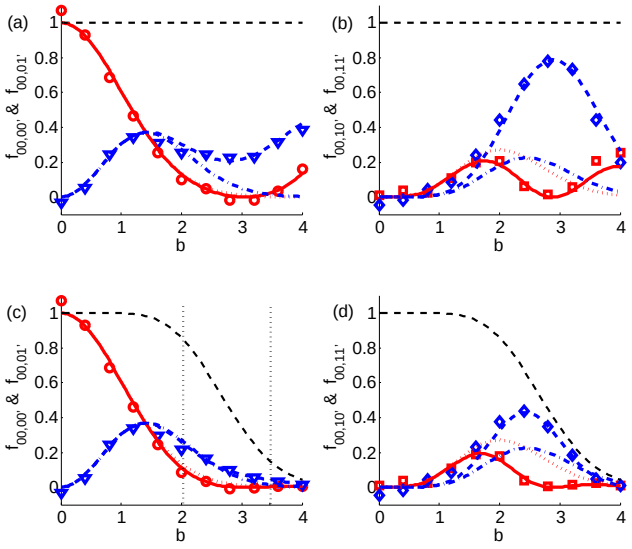

Figure 3.6: FCFs versus the displacement b. The experimental data points are indicated by symbols: circles ($f_{00,00'}$), triangles ($f_{00,01'}$), squares ($f_{00,10'}$), and diamonds ($f_{00,11'}$). The simulated FCFs for the 4-level system are shown by smooth lines ($f_{00,00'}$ and $f_{00,10'}$) and dashed lines ($f_{00,01'}$ and $f_{00,11'}$). The expected FCFs for infinite-level system are shown by dotted lines ($f_{00,00'}$ and $f_{00,10'}$) and dash-dotted lines ($f_{00,01'}$ and $f_{00,11'}$). The thin dashed lines at the top of each subplot corresponds to the normalization used. In (c), the thin vertical lines at $b = 2,\ 2\sqrt{3}$ mark the beginning of classically forbidden regions for $f_{00,00'}, f_{00,01'}$ respectively.

effect of truncation in the basis-set, and can be minimized by increasing the number of system qubits 3.3.

If one has the prior information on the normalization condition F, it is possible to get better agreement with the infinite case. This is illustrated in Figures 3.6c and 3.6d. The total probability for the first four levels in the infinite-level case varies with b as $\sum_j f_{00,j} = [1 + b^2/2 + b^4/8 + b^6/48]\, e^{-b^2/2}$ and is shown by thin-dashed lines at the top of Figures 3.6c and 3.6d. The experimental results with this normalization are shown by symbols. With the latter normalization both FCFs $f_{00,00'}$ and $f_{00,01'}$ show considerably good agreement with the infinite-level case, while the other levels still deviate significantly and require larger number of system qubits [14].

An interesting observation can be made by noting the non-zero

values of FCFs in classically forbidden regions. For example, for $f_{00,00'}$ ***and*** $f_{00,01'}$ ***(which match with the infinite theory), non-zero values respectively at*** $b \geq 2$ ***and*** $b \geq 2\sqrt{3}$ ***(shown by vertical dashed lines in Figure 3.6c) are due to overlap of tunneling amplitudes.***

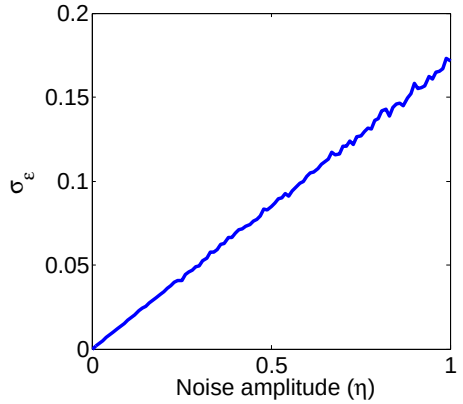

Figure 3.7: The average standard deviation of FCFs as a function of noise amplitude.

Finally to demonstrate the robustness of our protocol, we simulated FCFs by adding random noise to ancilla expectations. The average standard deviation $|\sigma_\epsilon\rangle$ of FCFs as a function of noise amplitude η is shown in Figure 3.7. It can be observed that $|\sigma_\epsilon\rangle < 0.2$ even at $\eta = 1$, indicating the robustness of the overall method.

3.3 Estimating FCFs using Method 2

Here we have used diagonal tomography to extract the expectation value of the observable.The observables here were $(P_{00}, P_{01}, P_{10}, P_{11})$.The system was initialized in elctronic ground state and using the translation operator U_T^k the excited electronic state was achieved,as explained in *section*3.2.After each translation,we extract the diagonal elements of the density matrix of the system by utilizing tomography.To estimate the FCFs only diagonal elements are sufficient as can be seen from the calculation below.
Suppose the systems density matrix at any time is ρ and our observable is

some projection operator $P = |n\rangle\langle n| = p_{ij}\delta_{in}\delta_{jn}$ with $p_{nn} = 1$.

$$\begin{aligned} \langle P \rangle &= Tr[\rho P] && (3.10)\\ &= Tr[\sum_{i,j} p_{ij}\delta_{in}\delta_{jn}\rho_{jk}] && (3.11)\\ &= p_{nn}\rho_{nn} && (3.12)\\ &= \rho_{nn} && (3.13) \end{aligned}$$

where, ρ_{nn} gives us the FCF corresponding to the initial state and the state $|n\rangle$. This implies that, we just need the diagonal element of the density matrix to find the $\langle P \rangle$,where depending on our choice of operator P and the initial state,we will get the overlap (and hence FCFs) between the corresponding wavefunctions.

3.3.1 Experiment

We chose three spin-1/2 F_{19} nuclei of iodotriflouroethylene(C_2F_3I) dissolved in acetone-D_6 as our 3-qubit NMR quantum processor.All the experiments are carried out on a 500MHz Brucker NMR spectrometer at an ambient temperatur of 300K. The molecular structure and the Hamiltonian parameters of our system is given in Figure 3.4.Since,we don't need an ancilla qubit here,our experiment here will correspond to the 3-qubit simulation in figure 3.3. Therefore,we're able to encode 8 lowest-levels of harmonic oscillator and hence obtained more FCF's than in method 1 with same number of qubits. In this way,this method is much efficient as it needs 1 less qubit than the method 1 to simulate the same problem.
The RF pulses for the translation operator are designed via GRAPE algorithm with an average Hilbert-Schmidt fidelity of 0.995 over a spatial RF inhomogeneity in the range of 90% to 110%. The results are shown in the figure3.8.

3.4 Conclusion

We described 2 general procedures for estimating Franck-Condon Factors (FCFs) in a quantum information processor.
1).First we observed that estimation of FCFs is equivalent to the measurement of certain projection operators on a set of qubits encoding the excited state of the system.We extended an existing method of measuring expectation value for this purpose.
2). We also estimated the FCFs using diagonal tomography approach which

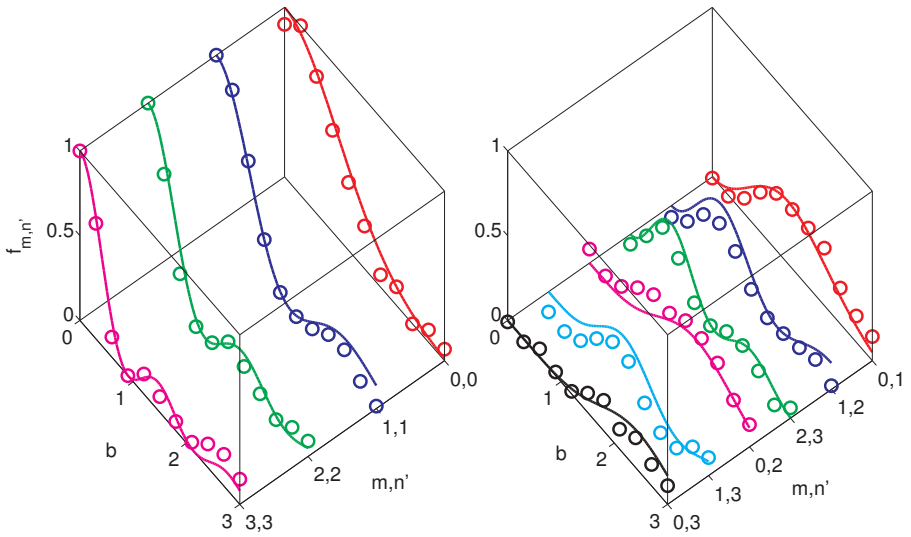

Figure 3.8: FCFs versus the displacement b. The experimental FCFs are represented by symbols(circles) and theoretical FCFs by solid lines.$|n\rangle$ denotes the elctronic ground state and $|n'\rangle$ denotes the elctronic excited state in number basis.**Left Cube** - it presents the $f_{0,0'}, f_{1,1'}, f_{2,2'}, f_{3,3'}$,where $f_{m,n'}$ represents the FCF for $|m\rangle and |n'\rangle$.**Right Cube** - it presents the FCFS for $f_{0,1}, f_{0,2}, f_{0,3}, f_{1,2}, f_{1,3}, f_{2,3}$. We can see that the experimental FCFs are in good qualitative agreement with the theoretical FCFs.

is much efficient than first approach in terms of resources needed,but first approach is much robust.
3) We were also able to show the non-zero overlap of wavefunctions in classically forbidden region,which is a direct implication of Quantum tunneling. We also noted that an excited state can be prepared by spatially translating the corresponding ground state. In general, if we have an arbitrary potential for the excited state, then it is still possible to prepare the final state using adiabatic evolutions.We illustrated these methods using a three qubit NMR quantum simulator and compared the results with the simulated curves for finite and infinite level systems. We demonstrated that even with only two/three qubits encoding the system, the FCFs corresponding to the lowest two/four levels still matched fairly well with the infinite-level theory.

References

[1] Brian Harold Bransden and Charles Jean Joachain. *Physics of atoms and molecules*. Pearson Education India, 2003.

[2] Boris V Chirikov and Dima L Shepelyansky. Correlation properties of dynamical chaos in hamiltonian systems. *Physica D: Nonlinear Phenomena*, 13(3):395–400, 1984.

[3] D. G. Cory, M. D. Price, and T. F. Havel. *Physica D*, 120:82, 1998.

[4] Wolfgang Demtroder. Atoms, molecules and photons. *Heidelberg, Springer-Verlag Berlin Heidelberg, 2006. 571*, 2006.

[5] Joseph Emerson, Yaakov S Weinstein, Seth Lloyd, and DG Cory. Fidelity decay as an efficient indicator of quantum chaos. *Physical review letters*, 89(28):284102, 2002.

[6] BM Fung. Use of pairs of pseudopure states for nmr quantum computing. *Physical Review A*, 63(2):022304, 2001.

[7] Fritz Haake. *Quantum signatures of chaos*, volume 54. Springer, 2010.

[8] Gerhard Herzberg. *Spectra of diatomic molecules*, volume 1. van Nostrand, 1950.

[9] Felix M Izrailev. Simple models of quantum chaos: spectrum and eigenfunctions. *Physics Reports*, 196(5):299–392, 1990.

[10] Navin Khaneja, Timo Reiss, Cindie Kehlet, Thomas Schulte-Herbrüggen, and Steffen J Glaser. Optimal control of coupled spin dynamics: design of nmr pulse sequences by gradient ascent algorithms. *Journal of Magnetic Resonance*, 172(2):296–305, 2005.

[11] Osama Moussa, Colm A Ryan, David G Cory, and Raymond Laflamme. Testing contextuality on quantum ensembles with one clean qubit. *Physical review letters*, 104(16):160501, 2010.

[12] Michael A Nielsen and Isaac L Chuang. *Quantum computation and quantum information*. Cambridge university press, 2010.

[13] Ivan Oliveira, Roberto Sarthour Jr, Tito Bonagamba, Eduardo Azevedo, and Jair CC Freitas. *NMR quantum information processing*. Elsevier, 2011.

[14] see supplementary material.

[15] Ramamurti Shankar. *Principles of quantum mechanics*, volume 233. Plenum Press New York, 1994.

[16] Abhishek Shukla, K Rama Koteswara Rao, and TS Mahesh. Ancilla-assisted quantum state tomography in multiqubit registers. *Physical Review A*, 87(6):062317, 2013.

[17] Hans-Jürgen Stöckmann. *Quantum chaos: an introduction*. Cambridge University Press, 2007.

[18] Dieter Suter and TS Mahesh. Spins as qubits: Quantum information processing by nuclear magnetic resonance. *The Journal of chemical physics*, 128(5):052206, 2008.

Appendix A

Proofs

A.0.1 Finding expectation value of a general unitary operator using Moussa protocol

Consider a general unitary operator U. To determine its expectation value we prepare the system in any desired state ρ, ancilla in state $|+\rangle$, and apply the Moussa protocol as shown in Fig. 3.2a. The state of the combined system evolves under the controlled-U operation as

$$|+\rangle\langle+| \otimes \rho \xrightarrow{U} \frac{1}{2}\left\{|0\rangle\langle 0| \otimes \rho + |0\rangle\langle 1| \otimes \rho U^\dagger + |1\rangle\langle 0| \otimes U\rho + |1\rangle\langle 1| \otimes U\rho U^\dagger\right\} \quad \text{(A.1)}$$

After tracing out system, the ancilla becomes

$$\frac{1}{2}\left\{|0\rangle\langle 0| + |0\rangle\langle 1|\langle U^\dagger\rangle + |1\rangle\langle 0|\langle U\rangle + |1\rangle\langle 1|\right\} = \begin{bmatrix} 1 & \langle U^\dagger\rangle \\ \langle U\rangle & 1 \end{bmatrix}. \quad \text{(A.2)}$$

In an NMR signal obtained with a quadrature detection, the real and imaginary parts correspond to the expectation values of σ_x and σ_y observables respectively [Ref]. Thus the real and imaginary parts of the ancilla signal are proportional to $\langle\sigma_x\rangle = \langle\frac{U+U^\dagger}{2}\rangle$ and $\langle i\sigma_y\rangle = \langle\frac{U-U^\dagger}{2}\rangle$, from which the expectation value $\langle U\rangle = \langle\sigma_x\rangle + i\langle\sigma_y\rangle$ can be extracted.

A.0.2 Extracting expectation value of a Hermitian operator compatible with a pure-state

The circuit for this measurement is shown in Figure 3.2c. Given the Hermitian operator A to be compatible with a pure state ρ, we can simultaneously diagonalize both of these using a similarity transformation U_s, i.e., $A_d = U_s^\dagger A U_s$, $\rho_d = U_s^\dagger \rho U_s$ are diagonal, and therefore $\langle A_d\rangle_{\rho_d} = \langle A\rangle_\rho$. As shown

above, the complex ancilla signal corresponds to $\langle\sigma_x\rangle_{\rm an} + i\langle\sigma_y\rangle_{\rm an} = \langle e^{iA_d\theta}\rangle_{\rho_d}$. In the following we prove that $\langle e^{iA_d\theta}\rangle_{\rho_d} = e^{i\langle A_d\rangle_{\rho_d}\theta}$. Since the system is in a pure state, we can write $\rho_d = |n\rangle\langle n|$ and $(\rho_d)_{ij} = \delta_{in}\delta_{jn}$. Now consider,

$$\begin{aligned}
\langle A_d^k\rangle_{\rho_d} &= \mathrm{Tr}\left[\rho_d A_d^k\right] \\
&= \sum_i (\rho_d A_d^k)_{ii} \\
&= \sum_{ij_1j_2\cdots j_k} \delta_{in}\delta_{j_1 n}(A_d)_{j_1 j_2}\cdots(A_d)_{j_k i} \\
&= (A_d)^k_{nn}, \quad \text{since } A_d \text{ is diagonal.}
\end{aligned} \tag{A.3}$$

For $k = 1$, we have $\langle A_d\rangle_{\rho_d} = (A_d)_{nn}$, and therefore $\langle A_d^k\rangle_{\rho_d} = \langle A_d\rangle^k_{\rho_d}$, which implies, $\langle e^{iA_d\theta}\rangle_{\rho_d} = e^{i\langle A_d\rangle_{\rho_d}\theta}$. Since $\langle A_d\rangle_{\rho_d} = \langle A\rangle_\rho$, we have $\langle\sigma_x\rangle_{\rm an} + i\langle\sigma_y\rangle_{\rm an} = e^{i\langle A\rangle_\rho\theta}$.